RSC Advances

PAPER

View Article Online
View Journal | View Issue

Check for updates

Cite this: *RSC Adv.*, 2021, **11**, 9955

A self-boosting microwave plasma strategy tuned by air pressure for the highly efficient and controllable surface modification of carbon†

Yanjing Liu,[a] Jiawei He,[a] Bing Zhang,[a] Huacheng Zhu,[a] Yang Yang,[a] Li Wu,[a] Wencong Zhang,*[b] Yanping Zhou *[a] and Kama Huang[a]

Surface modification is required to improve the activity and compositing ability of carbonaceous materials for their application in numerous areas such as energy storage, aerospace applications, and construction reinforcement. However, current strategies are facing problems such as the involvement of expensive and corrosive chemicals, poor controllability, and breakage of the carbon skeleton, thus sacrificing the mechanical and electrical properties. In this study, a green and controllable self-boosting microwave technology is proposed for the high-efficient surface modification of carbon. Air was used as the only oxidant. A carbon fiber cloth (CFC) is exposed to microwave irradiation in air for 90 s, yielding CFC with a surface oxygen content of 25.73%, 54.41%, and 52.56% at 1 atm, 8000 Pa, and 80 Pa, respectively, as determined *via* X-ray photoelectron spectroscopy. Notably, the content of each oxygen-containing functional group (*e.g.*, –C–OH and –C=O) is controllable by tuning the air pressure. Besides, CFC has enhanced mechanical and electrical properties. In comparison, CFC treated with a strong acid for 2 h only has a surface oxygen content of 21.4%, exhibiting greatly impaired electrical and mechanical properties. Numerical simulations at different pressures suggest that air plasma is triggered and boosted by the existence of CFC at 8000 Pa and 80 Pa, generating different electron number densities and electron temperature distributions, thus resulting in high-efficient and controllable modification.

Received 6th January 2021
Accepted 15th February 2021

DOI: 10.1039/d1ra00104c

rsc.li/rsc-advances

Open Access Article. Published on 08 March 2021. Downloaded on 9/14/2025 3:22:16 PM.
This article is licensed under a Creative Commons Attribution-NonCommercial 3.0 Unported Licence.

1. Introduction

Carbonaceous materials, harboring the merits of lightweight, rich micro/nano-structures and abundant precursors, have received tremendous research interest.[1–12] In numerous practical cases, the surface modification of carbon is required to improve its suspensibility, compositing capability, and activity. Among the carbonaceous materials, carbon fiber, due to its outstanding mechanical and electrical property and chemical stability, is emerging as a promising material in areas including energy storage[13–19] (*e.g.*, carbon fiber fabric/MnO_2 hybrid materials for efficient electrode materials of supercapacitors[13]), aerospace applications[14,20,21] (*e.g.*, carbon fiber-reinforced ultra-high temperature ceramic composites for engine propulsions[21]), construction reinforcement[22–24] (*e.g.*, reinforcement concrete beams using carbon fiber-reinforced polymers[22]), medical fields[14,25,26] (*e.g.*, carbon fiber-reinforced composite implants in orthopedic surgery[14]), and adsorption.[27–29] It can be seen that the application of carbon severely relies on its compositing capability with other materials. However, pristine carbonaceous materials are usually fabricated *via* high-temperature pyrolysis in an inert gas atmosphere,[30–33] which makes the surface of carbon extremely hydrophobic, hindering their application in numerous fields. For example, in the aerospace field, carbon fiber must be composited with other resins *via* interactions between active functional groups on the surface. Thus, it is urgently needed to develop an effective strategy for the surface modification of carbon products.

Currently, the main methods employed for the surface modification of carbon include gaseous oxidation by oxidizing gas such as ozone and wet or solid-phase chemical etching assisted by strong acid or alkali. These methods involve the use of numerous corrosive chemical reagents for hours,[34–36] which are costly and not desirable in green chemistry. Besides, the violent reaction conditions not only suffer from low efficiency and poor controllability but also damage the skeleton of carbon, thus sacrificing the mechanical and electrical properties of carbon. The green, effective, and controllable surface modification of carbonaceous materials remains challenging.

Plasma techniques have attracted considerable attention in the field of materials engineering, particularly in the modification of materials.[37–39] The plasma-processing strategy can help maintain the integrity of the structure of materials, and

[a]*College of Electronics and Information Engineering, Sichuan University, Chengdu 610065, China. E-mail: ypzhou11@scu.edu.cn; Tel: +86-18980850664*

[b]*School of Electronic and Communication Engineering, Guiyang University, Guiyang 550005, China. E-mail: zhangwencong89@126.com; Tel: +86-13408546852*

† Electronic supplementary information (ESI) available. See DOI: 10.1039/d1ra00104c

© 2021 The Author(s). Published by the Royal Society of Chemistry

Open Access Article. Published on 08 March 2021. Downloaded on 9/14/2025 3:22:16 PM.
This article is licensed under a Creative Commons Attribution-NonCommercial 3.0 Unported Licence.

distinctly enhance the wettability and electrochemical performance of materials.[38,39]

Recently, due to its unique heating characteristics (*i.e.*, fast heating, selective heating, and hot spots) derived from the dielectric loss-heating mechanism, microwave treatment has been found to shorten the reaction time and save energy significantly, and thus is very desirable for green chemistry. As such, microwave treatment has received tremendous research interest in the synthesis and modification of materials.[40–44] For example, Liu *et al.* thermally treated bamboo-based activated carbon using microwave radiation in N_2 for minutes, generating an activated carbon sample with increased C–O and less C=O, thus getting a better methylene blue adsorption performance.[45] However, most of the current work only applied microwave irradiation under atmospheric pressure. The feasibility of using air pressure to tune the treating effect of microwave irradiation is yet to be explored. In addition, no microwave field simulation has been studied to elucidate the mechanism of microwave treatment in this area.

In this study, a self-boosting microwave plasma strategy was developed for the high-efficient surface modification of carbon fiber cloth at sub-atmospheric pressures based on the strong interaction between carbon and microwave. Air was applied as the only oxidant. It was found that by tuning the air pressure, the content of total oxygen and each oxygen-containing functional group could be well controlled. Further microwave discharge simulation was done to give a possible explanation for the high-efficient and controllable surface modification.

2. Materials and methods

2.1. Materials

A carbon-fiber cloth (CFC, W0S 1009, 0.33 mm thick) was purchased from CeTech Co., Ltd, China. All chemicals were of analytical grade and used as received.

2.2. Surface modification of the carbon-fiber cloth *via* a self-boosting microwave strategy

A schematic illustration of the microwave reactor is shown in Fig. S1.† In a typical experiment, pristine CFC of 1 cm × 1 cm size was placed in a quartz tube sealed by a stainless-steel flange that was connected to a vacuum gauge and a pump. After the air pressure in the tube reached atmospheric pressure, 8000 Pa and 80 Pa, respectively, valve of the flange was closed. The tube was then placed vertically into the wave-guide cavity, and exposed to 500 W 2.45 GHz microwave irradiation. The input and reflected microwave powers were measured by power meters equipped on the double directional coupler. The position of the short-circuited plunger was tuned to minimize the reflected microwave power. The pictures and general temperature values of plasma were taken through the observation window (cut-off wave-guide) on the cavity. After 90 s, the microwave power was turned off and the quartz tube was naturally cooled to room temperature and taken out. The treated CFC samples were designated as CFC-atmosphere, CFC-8000 Pa, CFC-80 Pa, respectively. As a control, the pristine CFC was refluxed in a mixture of concentrated sulfuric acid and nitric acid at a volume ratio of 3 : 1 at 70 °C for 2 h and named as CFC-acid.

2.3. Characterization of the modified carbon fiber cloth

Static contact angles of the carbon fiber cloth surface were measured using the sessile drop method (Dataphysics OCA50, Germany). The morphology and elemental distribution of CFC were analyzed *via* field emission scanning electron microscopy (FESEM, EDS Mapping, Hitachi SU8020). The surface composition of CFC was analyzed *via* X-ray photoelectron spectroscopy (XPS, Thermo Escalab 250Xi). The atomic structural defect of CFC was analyzed on a Raman spectrometer (British Renishaw in *via*) with a semiconductor laser (λ = 532.0 nm) as an excitation source. The mechanical strength of CFC was measured using a universal material testing machine (Instron 5967, American). The electrical conductivity of CFC was measured by the four-probe method (KEITHLY MT2000).

2.4. Numerical simulation of microwave discharges

In order to figure out whether air plasma was created in the quartz tube, a mathematical model was proposed and corresponding numerical simulations were conducted to model microwave propagation, and air breakdown in the key part of the experimental setup (as shown in Fig. S2†) at different pressures. However, since modeling the microwave discharges in three dimensions involves a strongly nonlinear equation system, generally requiring an extremely dense mesh structure and an intolerably long computation time, reasonable simplifications and approximations are inevitable under our current conditions. It is worth noting that the following simplifications and approximations were applied in the numerical modelings of this study. (i) The calculation domain was simplified into two dimensions, as shown in Fig. S3,† whose validity has been explained in the ESI;† (ii) the CFC was assumed to be parallel to the *XY* plane; (iii) electric neutrality was assumed for the plasma and then the ambipolar diffusion approximation was used to simplify the equation system. (iv) The air plasma chemistry and the interactions between CFC and plasma particles were neglected. The details of the mathematical model are depicted in the ESI.†

3. Results and discussion

In this study, a microwave strategy in air was applied to modify the surface carbon fiber cloth (CFC) in a simple microwave-guided chamber based on a self-boosting strategy without the assistance of any external substance. Particularly, three pressure values were applied: atmospheric pressure, 8000 Pa, and 80 Pa. As shown in Fig. 1a–d, with the existence of CFC, only sparks were generated at atmospheric pressure; at 8000 Pa, bright yellow-white light was generated; at 80 Pa, the flame's color was purple-white. After 90 s of treatment, CFC samples were taken out and one drop of water was dropped onto them. It can be seen from Fig. 1e–h, CFC-pristine was extremely hydrophobic and exhibited a contact angle of 137.1°, while for each of the treated samples it was 0°, suggesting that the hydrophilic

© 2021 The Author(s). Published by the Royal Society of Chemistry

Open Access Article. Published on 08 March 2021. Downloaded on 9/14/2025 3:22:16 PM.
This article is licensed under a Creative Commons Attribution-NonCommercial 3.0 Unported Licence.

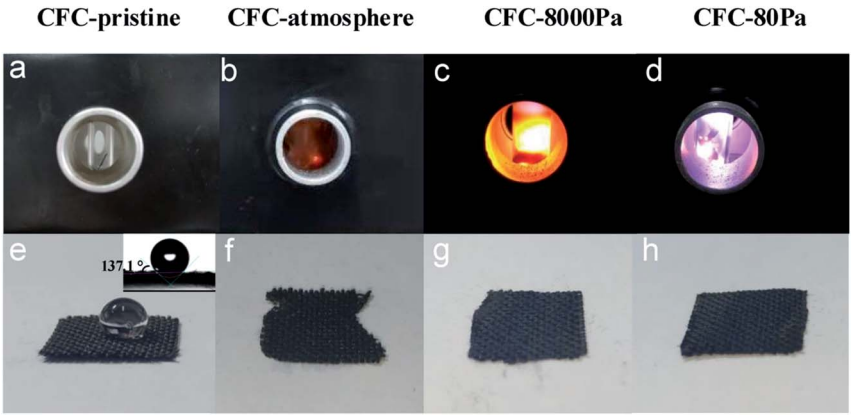

Fig. 1 Pictures of triggered plasma at different air pressures (a–d) and hydrophilicity testing results of the corresponding products (e–h). The inset in (e) is the contact angle of CFC-pristine.

modification of the CFC surface has been successfully realized under all pressures. However, while CFC treated at 8000 Pa and 80 Pa remained intact, the edge of the CFC treated at atmospheric pressure was severely combusted.

The XPS analysis was performed to characterize the generated functional groups, and the results are shown in Fig. 2. Fig. 2a shows the XPS spectra of the CFC samples, from which the atomic ratio (at%) of oxygen in each sample could be calculated, with the results listed in Table 1. CFC-pristine had a surface oxygen content of 5.73 at%, while the surface oxygen contents for CFC-atmosphere, CFC-8000 Pa, CFC-80 Pa and CFC-acid were 25.73 at%, 54.41 at%, 52.56 at% and 21.40 at%, respectively. This indicated that the microwave strategy was more efficient than the acid method in the surface modification of CFC, and sub-atmospheric pressures were more efficient than atmospheric pressure for the hydrophilic treatment under microwave irradiation. Notably, no peak for N 1s was observed, suggesting that there was almost no nitrogen content. Hence, nitrogen was not doped, which is consistent with the results of the plasma treatment in mixed gases containing N_2 in the literature.[46] The possible reason is that the ultraviolet radiation of air is very high, inhibiting the grafting of nitrogen.[46] Fig. 2b–f represent O 1s spectra of CFC-pristine, CFC-atmosphere, CFC-8000 Pa and CFC-80 Pa, CFC-acid, respectively. The O 1s peak

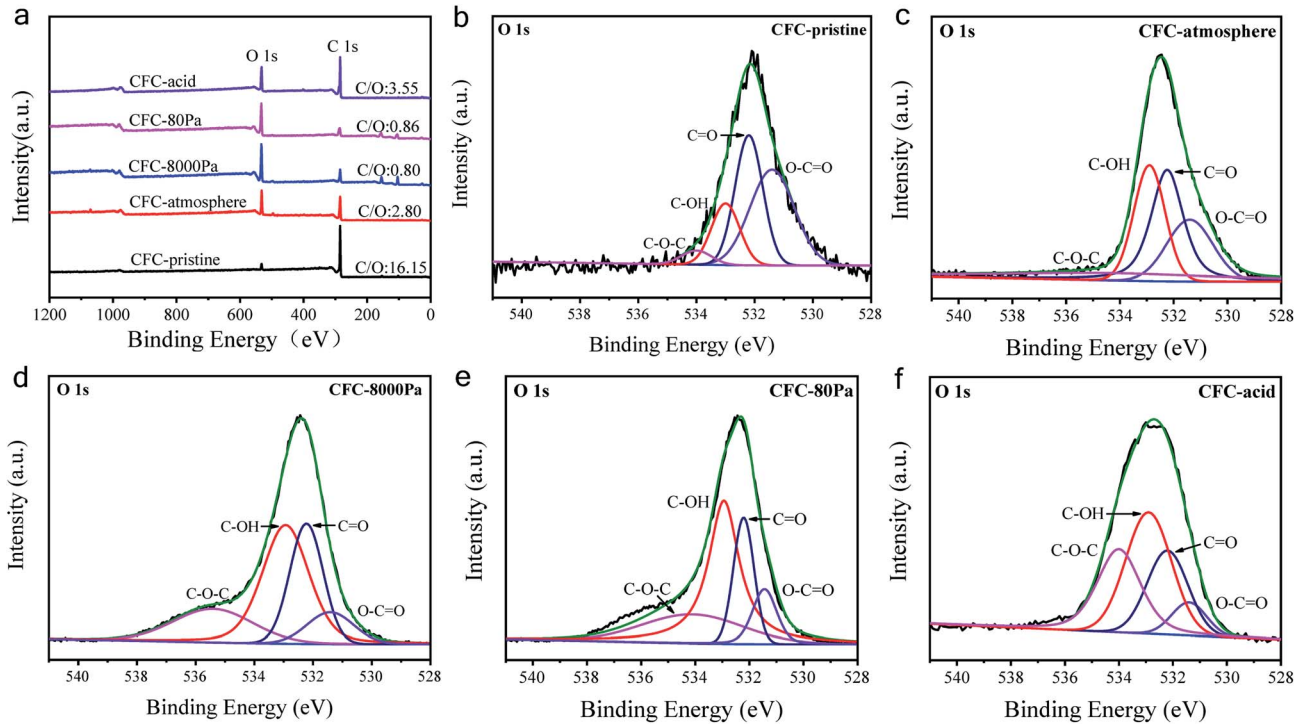

Fig. 2 (a) XPS spectra of carbon fiber samples; the O 1s spectra of (b) CFC-pristine, (c) CFC-atmosphere, (d) CFC-8000 Pa, (e) CFC-80 Pa, and (f) CFC-acid.

Open Access Article. Published on 08 March 2021. Downloaded on 9/14/2025 3:22:16 PM.
This article is licensed under a Creative Commons Attribution-NonCommercial 3.0 Unported Licence.

Table 1 Atomic ratio (at%) of oxygen and the percentage (%) of numerous oxygen-containing functional groups

(%)	CFC-pristine	CFC-atmosphere	CFC-8000 Pa	CFC-80 Pa	CFC-acid
O content	5.73	25.73	54.41	52.56	21.40
C–O–C	42.5	20.9	8.4	11.0	7.9
C=O	36.0	32.8	31.2	19.2	23.8
C–OH	17.3	26.9	30.6	48.2	38.7
O–C=O	4.2	19.4	29.8	21.6	29.6

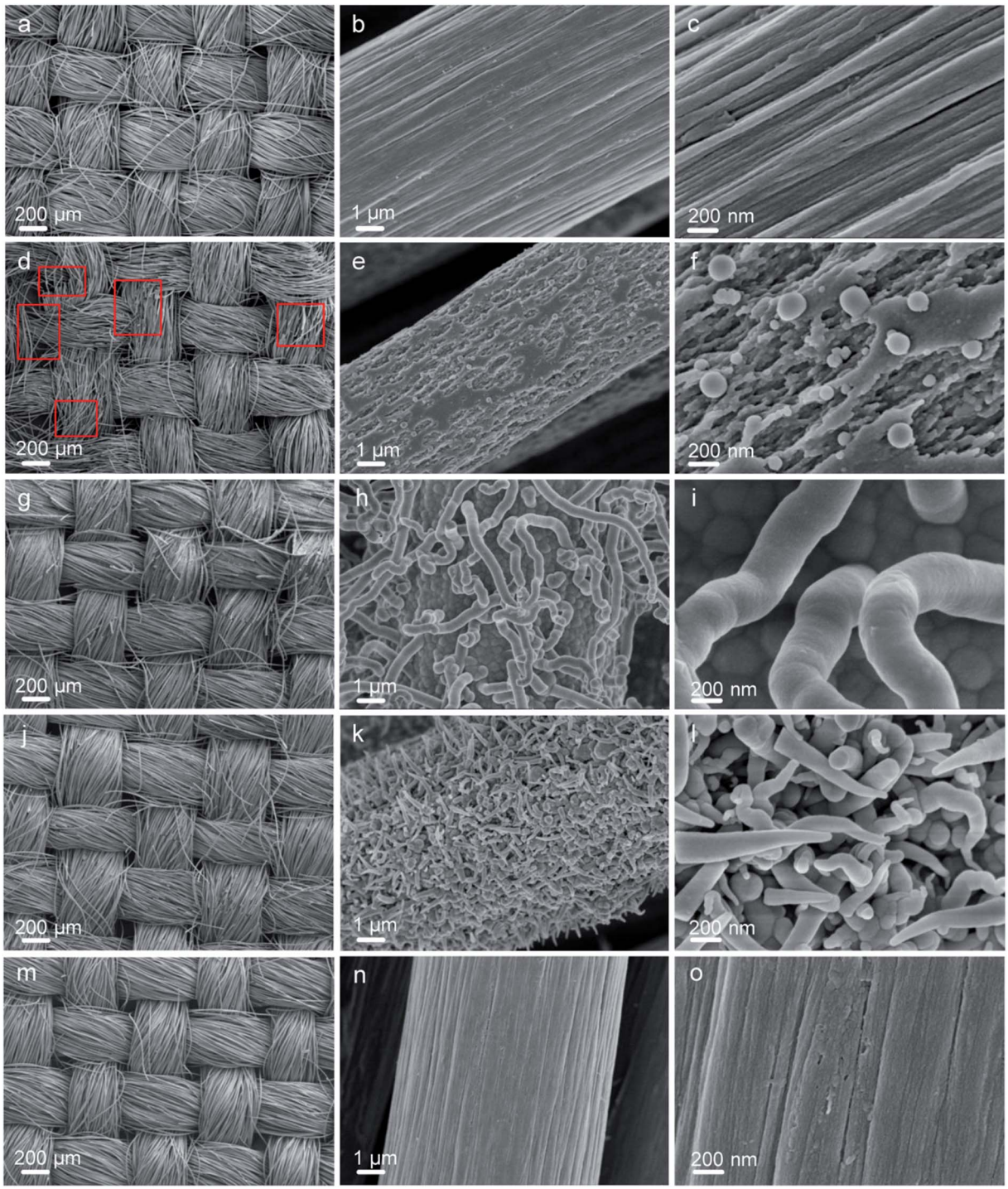

Fig. 3 FESEM images of CFC-pristine (a–c), CFC-atmosphere (d–f), CFC-8000 Pa (g–i), CFC-80 Pa (j–l), CFC-acid (m–o).

© 2021 The Author(s). Published by the Royal Society of Chemistry

Open Access Article. Published on 08 March 2021. Downloaded on 9/14/2025 3:22:16 PM.
This article is licensed under a Creative Commons Attribution-NonCommercial 3.0 Unported Licence.

could be divided into four peaks located at 531.4, 532.2, 532.9, and 534.0 eV, corresponding to C–O–C, C=O, C–OH, and O–C=O.[47–52] Among the four groups, the interacting capacity of C–OH and O–C=O with other materials is much higher than that of C–O–C and C=O. Hence, the percentages of these two functional groups are of particular interest. According to the area ratio of the four peaks, the percentage of each oxygen-containing functional group can be calculated. As shown in Table 1, C–OH and O–C=O contributed to 46.3%, 60.8%, 69.8% and 68.3% of the total oxygen content in CFC-atmosphere, CFC-8000 Pa, CFC-80 Pa and CFC-acid, respectively. This suggested that low working pressure was good for the production of the active groups. We found that atmospheric pressure was favorable for the production of C–O–C and C=O; 8000 Pa was beneficial for yielding C=O and O–C=O, and 80 Pa was the best for obtaining C–OH. As such, it is concluded that by tuning the reaction pressure, both the total oxygen content and each oxygen-containing group on the CFC surface could be tuned in the microwave strategy, illustrating the superiority of the microwave treatment.

The morphologies of the carbon fiber clothes were also examined. Compared to CFC-pristine (Fig. 3a–c), carbon fibers in the CFC-atmosphere were broken and the body was etched severely as indicated by the red boxes in Fig. 3d–f, which was consistent with the outlook picture of the sample in Fig. 1 and consistent with the literature.[53,54] At 8000 Pa, the carbon fibers were well maintained, and few carbon rods were generated on the fiber walls. At 80 Pa, the carbon fibers were not broken, but their surface carbon was transformed into a cone-like carbon. It is probably that the active particles in the plasma bombarded the carbon atoms on the carbon fiber, forming some carbon-containing active particles, which were chemically deposited to form cone-like carbon rods.[55] SEM-EDS mapping was conducted to examine the distribution of elemental O on the surface of CFC. It can be seen in Fig. S4† that little O was mapped out in CFC-pristine, while numerous O was distributed all around the surface of CFC-8000 Pa and CFC-80 Pa. The O contents were estimated to be 2%, 60% and 53%, respectively, which were quite in agreement with the quantitative results derived from XPS. Raman spectra of all the carbon fiber samples shown in Fig. 4a exhibit peaks at around 1350 cm^{-1} and 1600 cm^{-1}, which corresponded to the D band and G band of carbon.[56–60] The intensity ratio of the D band and G band (I_D/I_G) is an indicator of the graphitization degree of the carbon.[56–58] The smaller the I_D/I_G value, the more graphitized the carbon in the carbon fiber cloth is, which may be beneficial for better mechanical strength and electronic conductivity. CFC-pristine, CFC-atmosphere, CFC-8000 Pa and CFC-80 Pa had I_D/I_G values of 0.98, 1.08, 0.92 and 0.86, respectively. This indicated that the microwave treatment at 8000 Pa and 80 Pa increased the crystallinity of the carbon, while the treatment at atmospheric pressure led to more structural defects in the carbon crystal. The mechanical properties of all carbon fiber samples were characterized, and the results are shown in Fig. 4b and c. Compared to CFC-pristine, the tensile strength of CFC-atmosphere decreased by 40.1%, that of CFC-8000 Pa was

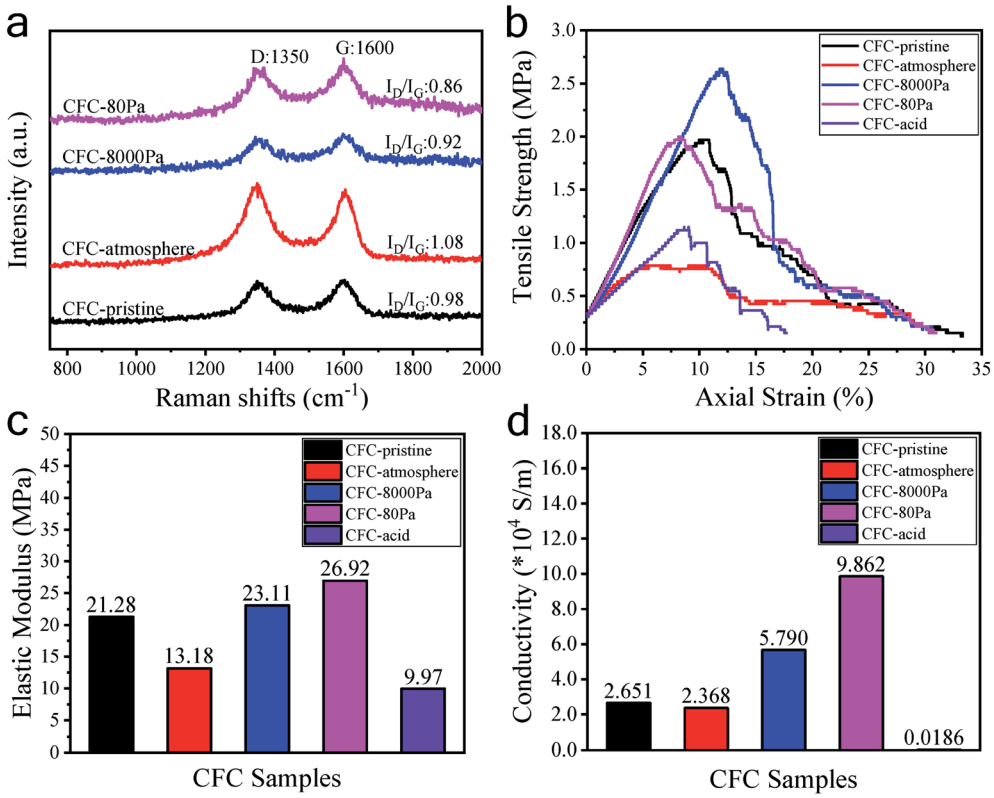

Fig. 4 Raman spectra (a), tensile strength values (b), elastic modulus values (c), and conductivity values (d) of the CFC samples.

Open Access Article. Published on 08 March 2021. Downloaded on 9/14/2025 3:22:16 PM.
This article is licensed under a Creative Commons Attribution-NonCommercial 3.0 Unported Licence.

enhanced by 34.0%, and that of CFC-80 Pa increased by 1.5%. The elastic modulus of CFC-atmosphere decreased by 38.1%, that of CFC-8000 Pa was enhanced by 8.6% and that of CFC-80 Pa increased by 26.5%. The decrease in the tensile strength of CFC-atmosphere was probably because of the broken fiber structure and etched microstructure, as indicated in FESEM images, and increased the disordered atomic carbon structure, as indicated by Raman spectra, which also resulted in a significant decrease in elastic modulus. Similarly, the enhanced tensile strength and elastic moduli of CFC-8000 Pa and CFC-80 Pa were regarded to be derived from the well-maintained continuous fiber structure, the newly formed surface microstructure and improved graphitic structure. The simultaneous improvement in the hydrophilic property and mechanical property of CFC was probably because the active substance in the air only hit the surface of the carbon fiber cloth, leading to an active surface and intact inner body. Moreover, the thermal effect of the microwave was able to reach and enhance the carbon skeleton. As a control, the tensile strength and elastic modulus of CFC-acid were demonstrated to decrease greatly, indicating the broken carbon skeleton during the fierce chemical reaction. The conductivities of the carbon fiber cloth samples were also characterized. As shown in Fig. 4d, the electronic conductivities of CFC-pristine, CFC-atmosphere, CFC-8000 Pa, CFC-80 Pa, and CFC-acid were 26 510, 23 680, 56 790, 98 620, and 186 S m^{-1}, respectively. After microwave treatments at 8000 Pa and 80 Pa, the electronic conductivities of samples were greatly enhanced. The reason was that the carbon fiber skeleton was not interrupted, as indicated in FESEM images, while the graphitization of carbon was improved, as indicated by Raman spectra.

In conclusion, based on the microwave-air technology, the surface of the carbon fiber cloth was successfully modified to have an oxygen content of 52.56% wherein C–OH and O–C=O accounted for 69.8%, while the mechanical and electrical properties of the carbon fiber cloth were simultaneously enhanced.

To figure out the mechanism of the microwave surface modification of CFC, a corresponding numerical simulation on the microwave discharges in the experimental setup was done. It can be seen from Fig. 5a that the incoming microwave was reflected and become a standing wave in the waveguide. Besides, electric field intensities in the areas on the left of the reacting tube were all significantly higher than those on the right of it, indicating that microwave was either reflected or dissipated in the quartz tube. When comparing the simulation results with and without the carbon fiber cloth, we found that at atmospheric pressure, the existence of the carbon fiber cloth contributed much, though not all, in affecting the microwave field distribution. However, at 8000 Pa and 80 Pa, the difference in the microwave field distribution with and without the carbon fiber cloth was small. The distribution of the microwave power dissipation shown in Fig. 5b indicates a strong interaction between CFC and microwave at $t = 0$ s. At $t = 1000$ ns, significant microwave power dissipation by CFC was still observed under 1 atm. However, no microwave power was dissipated by CFC under either 8000 Pa and 80 Pa. The simulation results suggested a strong interaction (dissipation) between the carbon

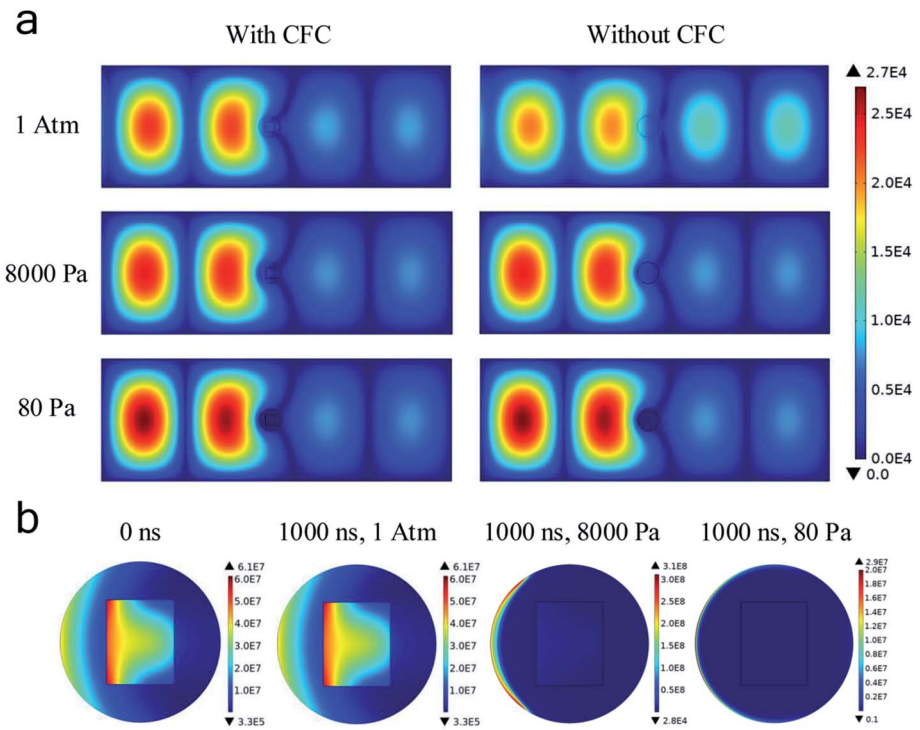

Fig. 5 (a) Distributions of the microwave electric field under different reacting conditions at the time of 1000 ns (unit: V m^{-1}); (b) distribution of microwave power dissipation at all pressures with CFC (unit: W m^{-3}).

© 2021 The Author(s). Published by the Royal Society of Chemistry

Open Access Article. Published on 08 March 2021. Downloaded on 9/14/2025 3:22:16 PM.
This article is licensed under a Creative Commons Attribution-NonCommercial 3.0 Unported Licence.

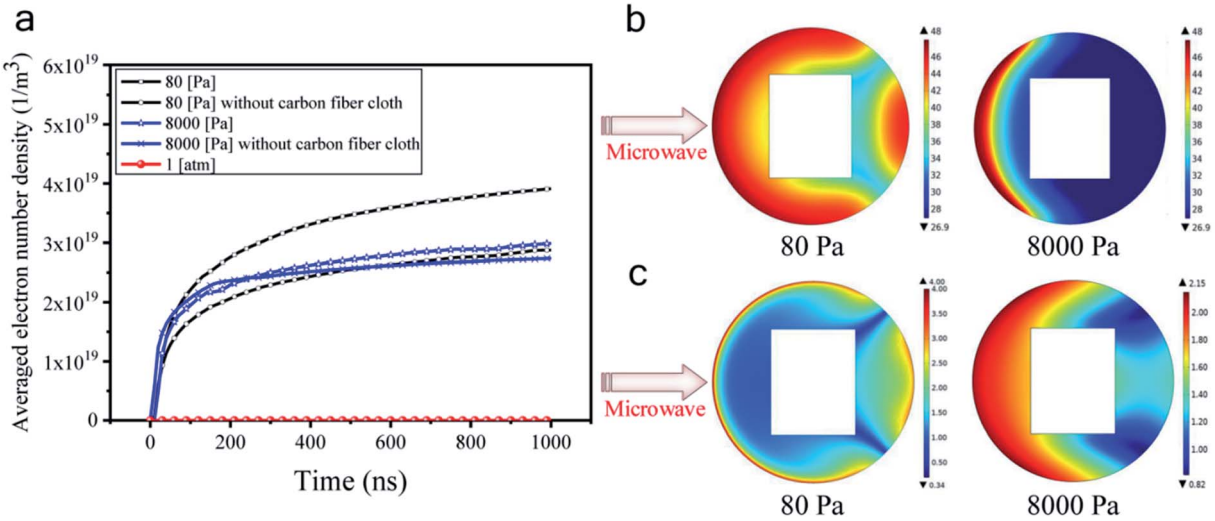

Fig. 6 (a) Variation of the averaged electron number density with time; (b) natural logarithm distribution of the electron number density ($\ln(n_e)$) at the time of 1000 ns (n_e is in the unit of m^{-3}); (c) distributions of electron temperature at the time of 1000 ns (unit: eV).

fiber cloth and microwave, and the air has probably been ionized, generating a large number of charged particles, thus shielding microwave from penetrating the tube and interacting with CFC directly at 8000 Pa and 80 Pa.

Fig. 6a shows that the averaged electron number density at atmospheric pressure did not increase with time. As such, the gas discharge was not triggered at atmospheric pressure at a microwave power of 500 W. However, at either 8000 Pa or 80 Pa, the electron number density rapidly exceeds 1×10^{19} m^{-3} within 100 ns, confirming that the microwave air breakdown occurred at these two pressures and gas discharge was successfully triggered to generate plasma. The mean-free path of electrons became long when the pressure became low, allowing enough time for the microwave electric field to accelerate electrons. Hence, microwave breakdown occurred under low pressures. Besides, it was found that electron number densities were generally higher in the presence of the carbon fiber cloth. For example, at 80 Pa, with the existence of the carbon fiber cloth, the averaged electron number density was about 4×10^{19} m^{-3} at 1000 ns, while that for the system without the carbon fiber cloth it was about 2.8×10^{19} m^{-3}. This suggested a boosting effect of the carbon fiber cloth. Based on this, it was believed that due to the self-boosting generation of plasma providing more active particles (*i.e.*, free electrons and radicals) at the two sub-atmospheric pressures, the surface oxygen contents of CFC-8000 Pa and CFC-80 Pa were much higher than that of CFC-atmosphere.

From Fig. 6a, we can also see that the averaged electron number density was calculated to be higher at 80 Pa than at 8000 Pa at all simulated times. To help understand the mechanism for the different modifying effects at 80 Pa and 8000 Pa, the distribution of the electron number density and the electron temperature is presented. Fig. 6b and c shows that the electron distributions were totally different under 80 Pa and 8000 Pa. In the carbon fiber cloth area, free electrons were more at 80 Pa than at 8000 Pa. However, the temperatures of electrons were comparable at 80 Pa and 8000 Pa. It is probable that the higher C–OH content and lower C=O and O–C=O contents in CFC-80 Pa than those in CFC-8000 Pa were caused by more active particles that were capable of creating more carbon active sites, which when reacting with air tend to form C–OH.[45]

4. Conclusion

In this study, a carbon fiber cloth was treated under microwave in air under three pressures. Through microwave simulation, we found that at 8000 Pa and 80 Pa, plasma was successfully triggered, giving yield to carbon fiber cloth's surfaces with more than 50% oxygen content. Moreover, the electronic and mechanical properties of the microwave-treated carbon fiber samples under these two sub-atmospheric pressures were enhanced simultaneously. Notably, the content of each oxygen-containing functional group could be tuned by the working pressure.

Author contributions

Yanjing Liu: methodology, investigation and writing-original draft preparation. Wencong Zhang: methodology, writing-reviewing and editing. Yanping Zhou: conceptualization, supervision, writing-reviewing, editing and funding acquisition. Jiawei He: discussion, validation. Bing Zhang: discussion, validation. Huacheng Zhu: discussion, validation. Yang Yang: discussion, validation. Li Wu: discussion, validation. Kama Huang: discussion, validation, funding acquisition.

Conflicts of interest

The authors declare that they have no known competing financial interests or personal relationships that could have appeared to influence the work reported in this paper.

© 2021 The Author(s). Published by the Royal Society of Chemistry

Open Access Article. Published on 08 March 2021. Downloaded on 9/14/2025 3:22:16 PM.
This article is licensed under a Creative Commons Attribution-NonCommercial 3.0 Unported Licence.

Acknowledgements

This work was financially supported by the National Natural Science Foundation of China (grant no. 61801314), National Natural Science Foundation of China (grant no. 61731013), Sichuan Science and Technology Program (grant no. 2019YFH0078), Fundamental Research Funds for the Central Universities of China (grant no. YJ201703), Young Scientific and Technological Talents Development Project from Guizhou Provincial Department of Education (grant no. QJHKYZ[2020] 087).

References

1 M. H. Shao, Q. W. Chang, J.-P. Dodelet and R. Chenitz, *Chem. Rev.*, 2016, **116**, 3594–3657.
2 L. Liu, H. P. Zhao and Y. Lei, *InfoMat*, 2019, **1**, 74–84.
3 Z. F. Yang, J. R. Tian, Z. F. Yin, C. J. Cui, W. Z. Qian and F. Wei, *Carbon*, 2019, **14**, 467–480.
4 H. Q. Zhao, Y. Chen, W. Liu, L. J. Yang, B. S. Zhang, L. Y. P. Wang, G. B. Ji and Z. C. J. Xu, *Nano-Micro Lett.*, 2019, **11**, 24.
5 Z. H. Wang, D. K. Shen, C. F. Wu and S. Gu, *Green Chem.*, 2018, **20**, 5031–5057.
6 C. M. Das, L. X. Kang, Q. L. Ouyang and K.-T. Yong, *InfoMat*, 2020, 1–17.
7 C. Delacou, I. Jeon, K. Otsuka, T. Inoue, A. Anisimov, T. Fujii, E. I. Kauppinen, S. Maru and Y. Matsuo, *InfoMat*, 2019, 1–12.
8 Z. H. Liu, B. G. Wang and L. X. Yu, *J. Energy Chem.*, 2018, **27**, 1369–1375.
9 D. X. Ji, L. Fan, L. L. Li, S. J. Peng, D. S. Yu, J. N. Song, S. Ramakrishna and S. J. Guo, *Adv. Mater.*, 2019, **31**, 1808267.
10 W. P. Yang, X. X. Li, Y. Li, R. M. Zhu and H. Pang, *Adv. Mater.*, 2018, 1804740.
11 Q. Liu, H. Q. Zhao, L. Li, P. P. He, Y. X. Wang, H. Y. Yang, Z. H. Hu and Y. Mu, *J. Hazard. Mater.*, 2018, **357**, 235–243.
12 S. J. Peng, L. L. Li, X. P. Han, W. P. Sun, M. Srinivasan, S. G. Mhaisalkar, F. Y. Cheng, Q. Y. Yan, J. Chen and S. Ramakrishna, *Angew. Chem., Int. Ed.*, 2014, **53**, 12594–12599.
13 M. Cakici, K. R. Reddy and M. F. Alonso, *Chem. Eng. J.*, 2017, **309**, 151–158.
14 N. Forintos and T. Czigany, *Composites, Part B*, 2019, **162**, 331–343.
15 J. J. Liang, C. C. Yuan, H. H. Li, K. Fan, Z. X. Wei, H. Q. Sun and J. M. Ma, *Nano-Micro Lett.*, 2018, **10**, 21.
16 Z. Li and B. H. J. Tang, *Green Chem.*, 2017, **19**, 5862–5873.
17 L. L. Li, S. J. Peng, H. B. Wu, L. Yu, S. Madhavi and X. W. Lou, *Adv. Energy Mater.*, 2015, **5**, 1500753.
18 Q. Yu, J. S. Lv, Z. H. Liu, M. Xu, W. Yang, K. A. Owusu, L. Q. Mai, D. Y. Zhao and L. Zhao, *Sci. Bull.*, 2019, **64**, 1617–1624.
19 S. J. Peng, G. R. Jin, L. L. Li, K. Li, M. Srinivasan, S. Ramakrishna and J. Chen, *Chem. Soc. Rev.*, 2016, **45**, 1225–1241.
20 J. G. Du, H. Z. Zhang, Y. M. Geng, W. Y. Ming, W. B. He, J. Ma, Y. Cao, X. K. Li and K. Liu, *Ceram. Int.*, 2019, **45**, 18155–18166.
21 S. F. Tang and C. L. Hu, *J. Mater. Sci. Technol.*, 2017, **33**, 117–130.
22 V. J. Ferrari, J. B. D. Hanai and R. A. D. Souza, *Constr. Build. Mater.*, 2013, **48**, 485–498.
23 B. G. Han, L. Q. Zhang, C. Y. Zhang, Y. Y. Wang, X. Yu and J. P. Ou, *Constr. Build. Mater.*, 2016, **125**, 479–489.
24 A. Feldhoff, E. Pippel and J. Woltersdorf, *Adv. Eng. Mater.*, 2000, **2**, 471–480.
25 D. J. Hak, C. Mauffrey, D. Seligson and B. Lindeque, *Orthopedics*, 2014, **37**, 825–830.
26 X. Mao, W. Tian, T. A. Hatton and G. C. Rutledge, *Anal. Bioanal. Chem.*, 2016, **408**, 1307–1326.
27 D. Cazorla-Amorós, J. Alcañiz-Monge and A. Linares-Solano, *Langmuir*, 1996, **12**, 2820–2824.
28 S. Senthilkumaar, P. R. Varadarajan, K. Porkodi and C. V. Subbhuraam, *J. Colloid Interface Sci.*, 2005, **284**, 78–82.
29 L. X. Tu, W. Z. Duan, W. L. Xiao, C. X. Fu, A. Q. Wang and Y. Zheng, *Sep. Purif. Technol.*, 2018, **192**, 30–35.
30 K. A. Khalid, A. A. Ahmad and T. L.-K. Yong, *J. Jpn. Inst. Energy*, 2017, **96**, 255–260.
31 G. Henrice-Olivé and S. Olivé, *Adv. Polym. Sci.*, 1983, **51**, 1–60.
32 A. Vedrtnam and S. P. Sharma, *Composites, Part A*, 2019, **125**, 105509.
33 S. J. Peng, L. L. Li, J. K. Y. Lee, L. L. Tian, M. Srinivasan, S. Adams and S. Ramakrishna, *Nano Energy*, 2016, **22**, 361–395.
34 Z. Y. Wu, Y. Y. Xu, X. L. Zhang, G. L. Shen and R. Q. Yu, *Talanta*, 2007, **72**, 1336–1341.
35 X. P. Zhang, L. Liu, M. Li, Y. J. Chang, L. Shang, J. L. Dong, L. H. Xiao and Y. H. Ao, *RSC Adv.*, 2016, **6**, 29428.
36 J. Li, *Surf. Interface Anal.*, 2009, **41**, 759–763.
37 B. Ouyang, Y. Zhang, X. Xia, R. S. Rawat and H. J. Fan, *Mater. Today Nano*, 2018, **3**, 28–47.
38 L. Tao, Q. Wang, S. Dou, Z. L. Ma, J. Huo, S. Y. Wang and L. M. Dai, *Chem. Commun.*, 2016, **52**, 2764–2767.
39 B. Ouyang, Y. Q. Zhang, Y. Wang, Z. Zhang, H. Jin Fan and R. Singh Rawat, *J. Mater. Chem. A*, 2016, **4**, 17801–17808.
40 D. Czylkowski, B. Hrycak, A. Sikora, M. Moczała-Dusanowska, M. Dors and M. Jasiński, *Materials*, 2019, **12**, 2418.
41 S. H. Yao, J. J. Zhang, D. K. Shen, R. Xiao, S. Gu, M. Zhao and J. Y. Liang, *J. Colloid Interface Sci.*, 2016, **463**, 118–127.
42 E. T. Kostas, D. Beneroso and J. P. Robinson, *Renew. Sustain. Energy Rev.*, 2017, **77**, 12–27.
43 S. Song, H. Yang, C. P. Su, Z. B. Jiang and Z. Lu, *Chem. Eng. J.*, 2016, **306**, 504–511.
44 C. L. Chen, B. Liang, A. Ogino, X. K. Wang and M. Nagatsu, *J. Phys. Chem.*, 2009, **113**, 7659–7665.
45 Q. S. Liu, T. Zheng, N. Li, P. Wang and G. Abulikemu, *Appl. Surf. Sci.*, 2010, **256**, 3309–3315.
46 U. Plawky, M. Londschien and W. Michaeli, *J. Mater. Sci.*, 1996, **31**, 6043–6053.
47 S. Huang, X. W. Cheng, X. Y. Guo, Y. Shi and W. Wang, *Appl. Surf. Sci.*, 2019, **497**, 143765.

© 2021 The Author(s). Published by the Royal Society of Chemistry

Open Access Article. Published on 08 March 2021. Downloaded on 9/14/2025 3:22:16 PM.
This article is licensed under a Creative Commons Attribution-NonCommercial 3.0 Unported Licence.

48 X. Z. Zhang, Y. D. Huang and T. Y. Wang, *Appl. Surf. Sci.*, 2006, **253**, 2885–2892.
49 L. M. Kong, X. B. Wang, W. Zheng, S. W. Tian, Y. Y. Qi, Y. J. Xue and B. C. Wang, *Mater. Res. Express*, 2020, **7**, 065304.
50 Y. P. Zhou, X. H. Zhang, Y. J. Liu, X. X. Xie, X. H. Rui, X. Zhang, Y. Z. Feng, X. J. Zhang, Y. Yu and K. M. Huang, *Small*, 2020, **26**, 1906669.
51 M. T. Zhao, X. B. Yan, L. Ren, M. L. Zhao, F. Guo, J. C. Zhuang, Y. Du and W. C. Hao, *InfoMat*, 2020, 1–8.
52 H. L. Chen, D. Yang, X. Y. Zhuang, D. Chen, W. L. Liu, Q. Zhang, H. H. Hng, X. H. Rui, Q. Y. Yan and S. M. Huang, *Nano Res.*, 2019, **13**, 1867–1874.
53 J.-M. Park, Z. Wang, D.-J. Kwon, G. Y. Gu, W.-I. Lee, J.-K. Park and K. L. De Vries, *Composites, Part B*, 2012, **43**, 2272–2278.
54 J. F. Xie, D. W. Xin, H. Y. Cao, C. T. Wang, Y. Zhao, L. Yao, F. Ji and Y. P. Qiu, *Surf. Coat. Technol.*, 2011, **206**, 191–201.
55 C. Zhang, L. S. Liu, Z. W. Xu, H. M. Lv, N. Wu, B. M. Zhou, W. Mai, L. H. Zhao, X. Tian and X. F. Guo, *Polym. Compos.*, 2018, **39**, E1262–E1268.
56 Q. J. Gong, H. J. Li, C. Z. Yao, S. Y. Zhang, K. Z. Li and C. Wang, *New Carbon Mater.*, 2013, **28**, 421–427.
57 Y.-K. Hsu, Y. C. Chen, Y. G. Lin, L.-C. Chen and K.-H. Chen, *J. Mater. Chem.*, 2012, **22**, 3383–3387.
58 S. S. Zance and S. Ravichandran, *Appl. Phys. A: Mater. Sci. Process.*, 2019, **125**, 456.
59 L. H. Zou, B. Y. Huang, Y. Huang, Q. Z. Huang and C. A. Wang, *Mater. Chem. Phys.*, 2003, **82**, 654–662.
60 L. B. Nohara, G. P. Filho, E. L. Nohara, M. U. Kleinke and M. C. Rezende, *Mater. Res.*, 2005, **8**, 281–286.

© 2021 The Author(s). Published by the Royal Society of Chemistry